Lateral Torsional Buckling of Steel W-Beams Subjected to Localized Fires

Chao Zhang[a,*], John L. Gross[a], Therese P. McAllister[a]

[a] *National Institute of Standards and Technology, 100 Bureau Drive, Stop 1070, Gaithersburg, MD 20899-1070, USA*

Abstract

Current design approaches to assess the lateral torsional buckling capacity of steel beams in fire are based on the assumption of uniform steel temperature. This paper investigates the effect of temperature gradients on the lateral torsional buckling behavior of steel wide flange (W) beams in fire conditions. The effects of localized fires and the temperature gradients they produce in steel beams were studied. Laterally unrestrained beams of various dimensions were subjected to a range of load ratios. The location of the localized fire was varied to provide different heating conditions. The standard ISO834 fire, and a uniform temperature condition in which the steel temperature was ramped linearly were used for comparison. The study shows that temperature gradients within a steel W-beam may have a detrimental effect on the lateral torsional buckling capacity of the beams in fire. The critical temperature, defined as the maximum temperature in a steel beam at which the beam undergoes lateral torsional buckling, in real fires may be hundreds of degrees lower than that in the standard ISO834 fire. The critical temperature in real

*Corresponding author. E-mail address: chao.zhang@nist.gov or 08_chao_zhang@tongji.edu.cn(C. Zhang)

fires may also be lower than that in the uniform heating condition. Design approaches based on the standard ISO834 fire or uniform steel temperature assumption may give unconservative results if the potential real fires are localized fires.
Keywords: Lateral torsional buckling; Steel beam; Localized fire; Critical temperature; Non-uniform temperature distribution; Numerical investigation

1. Introduction

Lateral torsional buckling (LTB) is a typical failure mode of steel beams. Although there have been many research studies on LTB of steel beams at ambient temperature, few studies have been conducted on LTB of steel beams under fire condition. Bailey et al. [1] numerically investigated the LTB of unrestrained steel beams with a uniform temperature distribution, and found that the design methods in both British and European codes over-predict the LTB resistance under fire condition. Vila-Real and Franssen [2] carried out a numerical study, and proposed a design method for LTB of steel beams with uniform temperature distributions. The design method was adopted in the Eurocode [3]. Vila-Real et al. [4] experimentally investigated the LTB of uniformly heated unrestrained steel beams. In their tests, the beam was heated from room temperature up to 600 ^{o}C and the mechanical loading was applied only after temperature stabilisation. The experimental data were used to validate the proposed method proposed by Vila-Real and Franssen [2]. Mesquita et al. [5] tested the LTB resistance of laterally unrestrained steel beams under uniform heating. In their tests, the mechan-

ical load was applied at room temperature and maintained constant during the heating process. The critical temperatures were recorded and compared with the predicted values from the simplified calculation procedure presented in Eurocode [3]. The simplified calculation procedure gave conservative results. Yin and Wang [6] numerically investigated the effect of non-uniform temperature distributions on LTB resistance of steel W-beams. In their studies, arbitrarily assumed non-uniform temperature distributions through the steel cross-section were considered. Only temperature variation through the section depth was considered and the assumed temperature profiles were uniform, linear, and bilinear. The temperature distribution across the section width, and along the member length was uniform. The study found that the critical temperatures of beams subjected to non-uniform temperature were higher than those subjected to uniform temperature.

Temperature distributions within steel components exposed to real fires may be highly non-uniform. Fig. 1 shows the temperature distribution within a steel beam exposed to flame impingement from a localized fire. In Fig. 1, because the fire source is located just below the beam center, the temperature distribution through the cross-section is symmetrical. In situations where the fire source is located away from the beam center line, the temperature distribution through the cross-section will be asymmetrical. In fact, for steel beams with three-sides exposed to the standard fire (i.e. top of beam protected by the floor slab), the temperature gradient within the cross-section is considerable [7, 8].

All previous studies on LTB of steel beams in fire, except [6], considered a uniform temperature distribution. The design methods adopted in current

codes to predict the LTB resistance are also based on the assumption of uniform temperature. This assumption gives conservative results only when the LTB resistance is governed by the steel strength at elevated temperature or by the magnitude of the mean temperature of the beam. However, it might give unconservative results when the temperature distribution within the steel beam is non-uniform and asymmetrical because of the secondary moment caused by thermal gradients [9]. In this paper, the LTB of simply supported laterally unrestrained steel W-beams subjected to localized fires was considered and the effect of highly non-uniform and asymmetrical temperature distribution on LTB resistance was investigated.

2. Methodology

2.1. Heat flux from localized fire

The correlations given in the SFPE handbook [10] are used to calculate the incident heat flux on different parts of a W-beam supporting a floor slab. The incident heat flux, $\dot{q}_{in}$, to the downward face of the lower flange is given by

$$\dot{q}_{in} = 518.8e^{-3.7y_B} \tag{1}$$

The incident heat flux to the upward face of the lower flange and the web is given by

$$\dot{q}_{in} = 148.1e^{-2.75y_C} \tag{2}$$

and the heat flux to the downward face of the upper flange is

$$\dot{q}_{in} = 100.5e^{-2.85y_C} \tag{3}$$

where y_i $(i = B, C)$ is a parameter given by

$$y_i = \frac{r + H_i + z_0}{L_i + H_i + z_0} \tag{4}$$

Here, r is the horizontal distance between the fire centerline and the calculated point along the beam; H_C and H_B are the distances between the fire and the ceiling, and the fire and the lower flange of the beam, respectively; L_B and L_C are the horizontal flame lengths along the lower and upper flanges of the W beam, calculated by

$$\frac{L_B + H_B}{H_B} = 2.3{Q^*_{H_B}}^{0.3} \tag{5}$$

and

$$\frac{L_C + H_C}{H_C} = 2.9{Q^*_{H_C}}^{0.4} \tag{6}$$

respectively; and z_0 is the vertical position of the virtual heat source given by

$$\frac{z_0}{D} = 2.4(1 - {Q^*_D}^{2/5}) \qquad (Q^*_D \geq 1.0) \tag{7a}$$

$$\frac{z_0}{D} = 2.4({Q^*_D}^{2/5} - {Q^*_D}^{2/3}) \quad (Q^*_D < 1.0) \tag{7b}$$

with

$$Q^*_D = \frac{\dot{Q}}{\rho_\infty c_p T_\infty \sqrt{g} D^{5/2}} \tag{8}$$

where, $\dot{Q}$ is the heat release rate (HRR) of the fire source; ρ_∞, c_p and T_∞ are density, specific heat and temperature of gas at ambient temperature; and g is the gravitational acceleration. In Eqs. 5 and 6, $Q^*_{H_B}$ and $Q^*_{H_C}$ are defined as in Eq. 8 only replacing D by H_B and H_C, respectively.

Eqs. 2 and 3 are valid for fires less than 2.0 MW. For fires greater than 2.0 MW, heat fluxes on all parts of the W-beam follow the correlation suggested

for the downward face of the lower flange provided in Eq. 1 (the constants in Eqs. 2 and 3 are replaced by the constants in Eq. 1).

2.2. Temperature of exposed steel I-beam

The temperature of an exposed steel W-beam is calculated by solving the three-dimensional (3D) heat conduction equation under the thermal boundary conditions for localized fires. The 3D heat conduction equation is given by

$$\nabla \cdot (k \nabla T) = \rho c \frac{\partial T}{\partial t} \tag{9}$$

where T is temperature; k, ρ, and c are thermal conductivity, density, and specific heat, respectively; and t is time.

The thermal boundary at an exposed surface is a Neumann boundary given by

$$-k \frac{\partial T}{\partial s}(0, t) = \dot{q}_{net} \tag{10}$$

where s denotes the inward normal direction; and $\dot{q}_{net}$ is the net heat flux transferred to the surface, calculated according to the Eurocode [11],

$$\dot{q}_{net} = \dot{q}_{in} - h_c(T_{surf} - 20) - \varepsilon_{res}\sigma[(T_{surf} + 273)^4 - (20 + 273)^4] \tag{11}$$

where h_c is the convective heat transfer coefficient, taken as 9 W/(m^{2}K) for localized fires [11]; T_{surf} is the surface temperature in unit of ^{o}C; ε_{res} is the resultant emissivity at the exposed surface; and $\sigma = 5.67 \times 10^{-8}$ W/(m^{2}K^4) is the Stefan-Boltzmann constant.

The thermal boundary at the end of the beam is assumed to be adiabatic.

2.3. High temperature steel properties

The T.T. Lie high temperature material model for steel [12] is used. The high temperature stress-strain relationship is given by

$$\sigma = \varepsilon E_T \quad (\varepsilon \leq \varepsilon_{pT}) \tag{12a}$$

$$\sigma = (12.5\varepsilon + 0.975) f_{yT} - \frac{12.5 {f_{yT}}^2}{E_T} \quad (\varepsilon > \varepsilon_{pT}) \tag{12b}$$

with

$$\varepsilon_{pT} = \frac{0.975 f_{yT} - 12.5 {f_{yT}}^2}{E_T - 12.5 f_{yT}} \tag{13}$$

where

$$\frac{E_T}{E_{20}} = 1.0 + \frac{T}{2000 In(T/1100)} \quad (T \leq 600\ ^oC) \tag{14a}$$

$$\frac{E_T}{E_{20}} = \frac{690 - 0.69T}{T - 53.5} \quad (600^oC < T \leq 1000\ ^oC) \tag{14b}$$

and

$$\frac{f_{yT}}{f_{y20}} = 1.0 + \frac{T}{900 In(T/1750)} \quad (T \leq 600\ ^oC) \tag{15a}$$

$$\frac{f_{yT}}{f_{y20}} = \frac{340 - 0.34T}{T - 240} \quad (600^oC < T \leq 1000\ ^oC) \tag{15b}$$

where σ and ε are stress and strain respectively; E_{20} and E_T are elastic modulus at room and elevated temperatures respectively; and f_{y20} and f_{yT} are yield strength and room and elevated temperatures respectively. In this study, the elastic modulus and yield strength at room temperature are $E_{20} = 2.06 \times 10^5$ MPa and $f_{y20} = 275$ MPa respectively.

The density, specific heat and thermal conductivity of the steel are taken as 7850 kg/m^3, 600 J/(kg K), and 45 W/(m K), respectively. The coefficient

of elongation of structural steel is given by

$$\alpha_s = (0.004T + 12) \times 10^{-6} \quad (20\ ^oC < T \leq 1000\ ^oC) \tag{16a}$$

$$\alpha_s = 1.6 \times 10^{-5} \quad (T \geq 1000\ ^oC) \tag{16b}$$

3. Numerical model

3.1. Description of the numerical model

The FEM program ANSYS [1] was used as the numerical tool. The applicability of ANSYS in structural fire analysis has been well documented in previous studies [7, 13, 14, 15, 16]. In this study, SHELL131 was used to predict the thermal behavior of steel W-beams in fire. SHELL131 is a 3D layered shell element having in-plane and through-thickness thermal conduction capability. It has 4 nodes with up to 32 temperature degrees of freedom at each node. The element is applicable to a 3D, steady-state or transient thermal analysis. SHELL131 generates temperatures that can be passed to structural shell elements (such as SHELL181) for structural analysis.

SHELL181 was used to predict the structural behavior of steel beams in fire. SHELL181 is suitable for analyzing thin to moderately-thick shell structures. It is a 4-node element with six degrees of freedom at each node: translations in the x, y, and z direction, and rotations about the x, y, and z

[1] Certain commercial entities, equipment, or materials may be identified in this document in order to describe an experimental procedure or concept adequately. Such identification is not intended to imply recommendation or endorsement by the National Institute of Standards and Technology, nor is it intended to imply that the entities, materials, or equipment are necessarily the best available for the purpose.

axes. SHELL181 is well-suited for linear, large rotation, and/or large strain nonlinear applications. Change in shell thickness is accounted for in nonlinear analysis.

3.2. Validation of the numerical model

In previous work [7], the capability of SHELL131 to solve the transient, nonlinear heat transfer problem was verified. In that paper, the capability of SHELL181 to predict the behavior of restrained steel beams exposed to fire was validated. This paper focuses on the suitability of SHELL181 to predict the LTB capacity of steel beams by comparing to both theory and test data.

In [1], the theoretical elastic LTB capacities of simply supported W-beams with a point load at the shear center of the section at the mid-span were used to verify a computer model. Table 1 gives the comparison between the FE predicted LTB results using SHELL181 and the reported theoretical values.

In [17], four tests were carried out to investigate the nonlinear LTB of simply supported steel W-beams at ambient temperature. Table 2 gives the comparison between the FE predictions using SHELL181 and the measured data.

In [5], tests on five beams with different span lengths and load ratios were carried out to investigate the LTB of unrestrained steel W-beams at high temperatures. The specimens were first loaded at ambient temperature, and then heated uniformly to critical temperatures at which LTB occurred. Table 3 gives the comparison between the FE results using SHELL181 and the measured critical temperatures.

In Tables 1 to 3, the predicted results agree reasonably well with the reported data, which validates SHELL181.

4. Case studies

4.1. Investigated cases

Laterally unrestrained simply supported steel W-beams subjected to flame impingement from localized fires were considered. Fig. 2 illustrates the model used in the study. The ceiling height was 2 m. The fire source was located at different positions on the floor and the heat release rate (HRR) followed a NFSC fire with maximum value of 1.6 MW, as shown in Fig. 3. The NFSC fire is assumed to be t-square in the growth stage and decay stage begins at the time when 70 percent of design fire load is consumed. In Fig. 3, the fire load density is 2000 MJ/m^2, the fire source area is 2 m^2, and the fire growth rate is 0.0117. The fire duration was 1 h. Table 4 gives the investigated cases. Two beams with different load ratios were considered. Beam 1 had a cross section 178 $\times$ 102 $\times$ 19UB and a clear span length of 2 m. Beam 2 had a cross section H250 $\times$ 250 $\times$ 8 $\times$ 12 and a clear span length of 4.5 m. The load ratio (μ_0) ranged from 0.3 to 0.9. Here, μ_0 is defined as the ratio of the applying bending moment to the bending moment capacity of the beam section calculated by design codes at ambient temperature. Uniform load, mid-span point load and point load at quarter length were considered, which were marked as "uniform" , "P at L/2" , and "P at L/4" in Table 4, respectively. The standard ISO834 fire and a uniform temperature condition in which the steel temperature was ramped linearly were considered for comparison, which were marked as "ISO834" and "unif" in Table 4, respectively. In the standard ISO834 fire, the steel beams were three sides exposed. In Table 4, $\triangle x$ denotes the distance between the flame axis and geometric center of the cross section, and $\triangle y$ denotes the distance between the flame axis

and the section having the maximum external moment. The term b_s denotes the beam width.

4.2. Steel temperature distribution

When a steel W-beam is subjected to a NFSC fire, the temperature distributions within the beam are highly non-uniform both across and along the beam, and the location of the maximum temperature changes with time. At the very beginning of the developing phase, the maximum temperature is located at the lower flange, as shown in Fig. 4a; then, the maximum temperature moves to the web and stays within the web during the later developing and steady burning phases, as shown in Fig. 4b and c; during the decay phase, the maximum temperature moves from the web to the upper flange, as shown in Fig. 4d.

When a steel W-beam is subjected to the ISO834 fire. The temperature distribution within the steel beam section is nonlinear. During the entire heating phase, the maximum temperature remains within the web (because web is thinner than flange).

4.3. Critical temperature

The numerical results for the critical temperature, T_{LTB}, which was defined as the maximum temperature in a steel beam at which LTB occurs, were also provided in Table 4.

When the fire source is near the geometric center of the section, or when $\triangle x$ is small, the T_{LTB} for the NFSC fire is higher than that for the standard fire, and the "unif" temperature gives the lowest T_{LTB}. However, when $\triangle x$ is large, the T_{LTB} for the NFSC fire will be lower than that for the standard

fire, and the maximum difference can be as high as 161 ^{o}C (491-330=161 ^{o}C, for case 6-6). When $\triangle x$ is large, in most cases the "unif" temperature gives the lowest T_{LTB}, and in some cases, T_{LTB} in the NFSC fire can be lower than that in the "unif" temperature.

Fig. 5 shows that the T_{LTB} for the NFSC fire decreases with increasing $\triangle x$. Fig. 6 shows that the T_{LTB} for the NFSC fire increases with the increasing of $\triangle y$.

It should be noted that when $\triangle x$ is large enough (i.e. far from the beam centerline), LTB will not occur.

5. Discussions

5.1. Failure criteria

A laterally unrestrained beam can maintain its stability when the external moment caused by the applied load, M, is less than a critical internal moment, M_{crit}, thus

$$M < M_{crit} \tag{17}$$

The critical internal moment is determined by the dimensions of the beam, loading and end restraint conditions, point of load application, and the material properties at elevated temperature. For a laterally unrestrained simply supported W-beam, the elastic critical moment is calculated by [18]

$$M_{crit} = C_1 \frac{\pi^2 E I_z}{L^2} [\sqrt{\frac{I_w}{I_z} + \frac{L^2 G I_t}{\pi^2 E I_z} + (C_2 z_g)^2} - C_2 z_g] \tag{18}$$

where, C_1 and C_2 are coefficients depending on the loading and end restraint conditions; E and G are Young modulus and shear modulus respectively; I_z, I_t and I_w are second moment of area about the weak axis, torsional constant

and warping constant respectively; L is beam length; and z_g is distance between the point of load application and the shear center, as shown in Fig. 7. In the general case z_g is positive for loads acting towards the shear center from their point of application, and the larger z_g, the smaller the M_{crit}.

5.2. Average steel temperature

Fig. 8 shows the effect of $\triangle x$ on temperature distribution in a beam. In Fig. 8, the maximum steel temperatures for different $\triangle x$ are equal and taken as 300 ^{o}C. For a given maximum steel temperature, the temperature distribution in a beam is more uniform for a larger $\triangle x$ than for a smaller $\triangle x$, and the temperatures in most parts of the beam are higher for a larger $\triangle x$ than for a smaller $\triangle x$. Since a beam with a much more uniform temperature distribution and higher average temperature has less strength and stiffness (and smaller I_z, I_t and I_w) than the beam with the same maximum temperature but less uniform temperature distribution, for a given load and end restraint conditions, and ignoring the effect of temperature gradient on the location of shear center, T_{LTB} for a beam with more uniform temperature distribution is lower than the beam with less uniform temperature distribution. As a result, T_{LTB} decreases with increasing of $\triangle x$, as shown in Fig. 5.

Depending on the value of $\triangle x$ and the specified moment, the average temperature of a beam subjected to a NFSC fire can be higher or lower than that of the beam with the same maximum temperature but subjected to the standard ISO834 fire. For cases with small $\triangle x$, when a beam occurs LTB in the standard ISO834 fire, the beam with the same maximum steel temperature in the NFSC fire is able to resist further temperature rising because of the lower average temperature; similarly when a beam occurs

LTB in a NFSC fire with a large $\triangle x$, the beam with the same maximum steel temperature in the standard ISO834 fire is also able to resist further temperature rising.

Fig. 9 shows the temperature distributions within different parts of beam 1 subjected to a NFSC fire, and the standard ISO834 fire. In Fig. 9, the maximum steel temperatures for those two fires are equal and taken as 503 ^{o}C which is the critical temperature in the standard ISO834 fire. Due to a lower average temperature, the beam in the NFSC fire does not fail when its maximum temperature reach 503 ^{o}C and will fail at a critical temperature of 603 ^{o}C. Fig. 10 shows the temperature distributions within different parts of beam 1 subjected to another fire, and the standard ISO834 fire. In Fig. 10, the maximum steel temperatures for those two fires are equal and taken as 429 ^{o}C which is the critical temperature in the NFSC fire. For the upper flange, temperatures near the beam center are higher for the NFSC fire than for the standard ISO834 fire, whilst temperatures far from the beam center are lower for the NFSC fire than for the standard ISO834 fire. For the lower flange, temperatures are much higher for the NFSC fire than for the standard ISO834 fire (the difference can reach 105 ^{o}C). For the web, temperatures are mostly lower for the NFSC fire than for the standard ISO834 fire. Therefore because temperatures in most parts of the beam in the standard ISO834 fire are lower than those in the NFSC fire, the beam in the standard fire does not fail when its maximum temperature reach 429 ^{o}C and will fail at a critical temperature of 503 ^{o}C.

For a given maximum steel temperature, the average temperature of a steel beam in the standard ISO834 fire is lower than that of the beam in

uniform temperature. Therefore, the critical temperature for the standard fire is higher than that for the uniform temperature.

5.3. Temperature gradient

Temperature gradient in beam section has effect of changing shear center. For cases 5-11 and 6-6, beams in the NFSC fire occur LTB in the cooling phase but do not occur LTB at the same maximum steel temperatures in the heating phase, as shown in Figs. 11 and 12. In Figs. 11 and 12, the maximum temperatures are located at the upper flange in the cooling phase and at the web in the heating phase, and the shear centers are lower in the cooling phase. Due to the lower shear centers or larger z_g, the beams survive the heating phase but fail in the cooling phase.

Therefore, although for a given maximum steel temperature the average temperature of a steel beam in a NFSC fire is always lower than that of the beam in uniform temperature, for some cases in which the effect of temperature gradient is so great, the T_{LTB} of a beam in a NFSC fire can be lower than that in uniform temperature, as for cases 5-11 and 6-6.

6. Conclusions

The lateral torsional buckling of steel I-beams subjected to localized fires have been investigated numerically using ANSYS. Based on the results of this investigation, the following conclusions can be drawn:

- The critical temperature at which a beam fails by lateral torsional buckling in a real fire may be hundreds of degrees lower than that resulting from the standard fire. The critical temperature in a real fire may also be lower than that under uniform heating condition.

- The temperature gradient within the steel beam may have a negative effect on the torsional buckling capacity of steel I-beams in fire, which is opposite to the findings by other researchers who use arbitrary temperature distributions in their study.

- The location of the fire source has a significant effect on the lateral torsional buckling of steel W-beams in localized fires.

- The critical temperature in the standard fire is higher than that in a uniform heating condition.

- Structural fire design based on the standard fire may be unconservative when there exists the potential for a localized fire with flame impingement on the structural element.

[1] C.G. Bailey, I.W. Burgess, R.J. Plank. The lateral-torsional buckling of unrestrained steel beams in fire. Journal of Constructional Steel Research, 1996;36:101-19.

[2] P.M.M. Vila-Real, J.-M. Franssen. Numerical modelling of lateral buckling of steel I beams under fire-conditions - comparsion with Eurocode 3. Journal of Fire Protection Engineering, 2001;11:112-28.

[3] European Committee for Standardisation (CEN). ENV 1993-1-2, Eurocode 3 Design of steel structures. Part 1.2 General rules/structural fire design. British Standards Institution, London, 2001.

[4] P.M.M. Vila-Real, P.A.G. Piloto, J.-M. Franssen. A new proposal of a simple model for the lateral-torsional buckling of unrestrained steel I

beams in case of fire: experimental and numerical validation. Journal of Constructional Steel Research, 2003;59:179-99.

[5] L.M.R. Mesquita, P.A.G. Piloto, M.A.P. Vaz, PMM Vila-Real. Experimental and numerical research on the critical temperature of laterally unrestrained steel I beams. Journal of Constructional Steel Research, 2005;61:1435-46.

[6] Y.Z. Yin, Y.C. Wang. Numerical simulations of the effects of non-uniform temperature distributions on lateral torsional buckling resistance of steel I-beams. Journal of Constructional Steel Research, 2003;59:1009-33.

[7] C. Zhang, G.Q. Li, A Usmani. Simulating the Behavior of Restrained Steel Beams to Flame Impinged Localized Fires. Journal of Constructional Steel Research, 2013;83:156-65.

[8] J. Kruppa, B. Zhao. Fire resistance of composite beams to Eurocode 4 Part 1.2. Journal of Constructional Steel Research, 1995;33:51-69.

[9] A.S. Usmani, J.M. Rotter, S. Lamont, A.M. Sanad, M. Gillie. Fundamental principles of structural behavior under thermal effects. Fire Safety Journal, 2001;36:721-44.

[10] B.Y. Lattimer. Heat fluxes from fires to surfaces. In: SFPE Handbook of Fire Protection Engineering, 3rd edition, Section 2-4, Society of Fire Protection Engineers, Maryland, 2002.

[11] Eurocode 1: Actions on structures - Part 1-2: General actions - Actions on structures exposed to fire. BSI, 2002.

[12] T. T. Lie, B.A. Macaulay. Evaluation of the fire resistance of protected steel columns. Internal Report No. 583, National Research Concil Canada; 1989.

[13] G.Q. Li, C. Zhang. Creep effect on buckling of axially restrained steel columns in real fires. Journal of Constructional Steel Research, 2012;71:182-8.

[14] C. Zhang, G.Q. Li, Y.C. Wang. Sensitivity study on using different formulae for calculating the temperature of insulated steel members in natural fires. Fire Technology, 2012;48:343-66.

[15] G.Q. Li, C. Zhang. Thermal response to fire of uniformly insulated steel members: background and verification of the formulation reccomended by chinese code CECS200. Advanced Steel Construction, 2010;6:788-802.

[16] G.Q. Li, C. Zhang. Simple approach for calculating maximum temperature of insulated steel memebrs in natural-fires. Journal of Constructional Steel Research, 2012;71:104-11.

[17] S Kitipornchai, NS Trahair. Inelastic buckling of simply supported steel I-beams. Journal of the Structural Division, ASCE 1975;101:1333-47.

[18] SN003a-EN-EU. NCCI:Elastic critical moment for lateral torsional buckling, 2008.

Table 1: Comparison between FE predictions and the elastic theoretical results reported by Bailey et al. [1]

Section	Span (m)	Theoretical (kN)	Predicted (kN)	Error (%)
$686 \times 254 \times 125$UB	8.0	390.41	383.52	-1.76
$533 \times 210 \times 82$UB	8.0	154.20	159.52	3.45
$406 \times 178 \times 54$UB	6.0	136.77	137.40	0.46

Table 2: Comparison between FE predictions and ambient temperature test reported by Kitipornchai and Trahair [17]

Section	Span (m)	Measured (kN)	Predicted (kN)	Error (%)
10UB29	2.44	234.96	258.97	10.22
	3.05	185.12	195.55	5.63
	3.66	145.07	151.05	4.12
	6.10	56.96	62.47	9.67

Table 3: Comparison between FE predictions and elevated temperature test reported by Mesquita et al. [5]

Section	Span	Measured (^{o}C)	Predicted (^{o}C)	Error (%)
IPE100	1.5	704	717	1.85
	2.0	680	710	4.41
	2.5	737	710	-3.66
	3.5	717	729	1.67
	4.5	748	760	1.60

Table 4: Investigated cases

Case	beam	Load type	μ_0	$\triangle x$ (m)	$\triangle y$ (m)	Fire	T_{LTB} ^{o}C
1-1	#1	uniform	0.3	0	0	NFSC	794
1-2	#1	uniform	0.3	$3.5b_s$	0	NFSC	725
1-3	#1	uniform	0.3	$5.5b_s$	0	NFSC	686
1-4	#1	uniform	0.3	$7.5b_s$	0	NFSC	NO[2]
1-5	#1	uniform	0.3	0	$L/4$	NFSC	802
1-6	#1	uniform	0.3	-	-	iso834	695
1-7	#1	uniform	0.3	-	-	unif	659
2-1	#1	uniform	0.5	0	0	NFSC	727
2-2	#1	uniform	0.5	$3.5b_s$	0	NFSC	674
2-3	#1	uniform	0.5	$5.5b_s$	0	NFSC	646
2-4	#1	uniform	0.5	$7.5b_s$	0	NFSC	617
2-5	#1	uniform	0.5	$9.5b_s$	0	NFSC	586
2-6	#1	uniform	0.5	$15.5b_s$	0	NFSC	NO
2-7	#1	uniform	0.5	0	$L/4$	NFSC	758
2-8	#1	uniform	0.5	-	-	iso834	611
2-9	#1	uniform	0.5	-	-	unif	532
3-1	#1	uniform	0.7	0	0	NFSC	603
3-2	#1	uniform	0.7	$3.5b_s$	0	NFSC	569
3-3	#1	uniform	0.7	$5.5b_s$	0	NFSC	556

[2]LTB not happen

Table 4: (continued)

Case	beam	Load type	μ_0	$\triangle x$ (m)	$\triangle y$ (m)	Fire	T_{LTB} ^{o}C
3-4	#1	uniform	0.7	$7.5b_s$	0	NFSC	539
3-5	#1	uniform	0.7	$9.5b_s$	0	NFSC	519
3-6	#1	uniform	0.7	$15.5b_s$	0	NFSC	452
3-7	#1	uniform	0.7	$17.5b_s$	0	NFSC	429
3-8	#1	uniform	0.7	0	$L/4$	NFSC	675
3-9	#1	uniform	0.7	0	$L/8$	NFSC	625
3-10	#1	uniform	0.7	-	-	iso834	503
3-11	#1	uniform	0.7	-	-	unif	390
4-1	#1	uniform	0.8	0	0	NFSC	502
4-2	#1	uniform	0.8	$3.5b_s$	0	NFSC	484
4-3	#1	uniform	0.8	$5.5b_s$	0	NFSC	475
4-4	#1	uniform	0.8	$7.5b_s$	0	NFSC	467
4-5	#1	uniform	0.8	$9.5b_s$	0	NFSC	455
4-6	#1	uniform	0.8	$15.5b_s$	0	NFSC	403
4-7	#1	uniform	0.8	$17.5b_s$	0	NFSC	385
4-8	#1	uniform	0.8	$19.5b_s$	0	NFSC	363
4-9	#1	uniform	0.8	$21.5b_s$	0	NFSC	345
4-10	#1	uniform	0.8	$23.0b_s$	0	NFSC	332
4-11	#1	uniform	0.8	$23.4b_s$	0	NFSC	312
4-12	#1	uniform	0.8	$23.5b_s$	0	NFSC	NO
4-13	#1	uniform	0.8	-	-	iso834	424

Table 4: (continued)

Case	beam	Load type	μ_0	$\triangle x$ (m)	$\triangle y$ (m)	Fire	T_{LTB} ^{o}C
4-14	#1	uniform	0.8	-	-	unif	292
5-1	#1	uniform	0.9	0	0	NFSC	354
5-2	#1	uniform	0.9	$22.5b_s$	0	NFSC	260
5-3	#1	uniform	0.9	$23.5b_s$	0	NFSC	256
5-4	#1	uniform	0.9	$24.5b_s$	0	NFSC	246
5-5	#1	uniform	0.9	$25.5b_s$	0	NFSC	241
5-6	#1	uniform	0.9	$26.5b_s$	0	NFSC	232
5-7	#1	uniform	0.9	$27.5b_s$	0	NFSC	231
5-8	#1	uniform	0.9	$29.5b_s$	0	NFSC	218
5-9	#1	uniform	0.9	$30.5b_s$	0	NFSC	209
5-10	#1	uniform	0.9	$31.0b_s$	0	NFSC	199
5-11	#1	uniform	0.9	$31.2b_s$	0	NFSC	180
5-12	#1	uniform	0.9	$31.3b_s$	0	NFSC	NO
5-13	#1	uniform	0.9	-	-	iso834	302
5-14	#1	uniform	0.9	-	-	unif	181
6-1	#1	P at $L/2$	0.7	0	0	NFSC	571
6-2	#1	P at $L/2$	0.7	$17.5b_s$	0	NFSC	420
6-3	#1	P at $L/2$	0.7	$19.5b_s$	0	NFSC	398
6-4	#1	P at $L/2$	0.7	$20.5b_s$	0	NFSC	360
6-5	#1	P at $L/2$	0.7	$21.0b_s$	0	NFSC	335
6-6	#1	P at $L/2$	0.7	$21.1b_s$	0	NFSC	330

Table 4: (continued)

Case	beam	Load type	μ_0	$\triangle x$ (m)	$\triangle y$ (m)	Fire	T_{LTB} ^{o}C
6-7	#1	P at $L/2$	0.7	$21.2b_s$	0	NFSC	NO
6-8	#1	P at $L/2$	0.7	0	$L/4$	NFSC	705
6-9	#1	P at $L/2$	0.7	0	$L/8$	NFSC	632
6-10	#1	P at $L/2$	0.7	-	-	iso834	491
6-11	#1	P at $L/2$	0.7	-	-	unif	339
7-1	#1	P at $L/4$	0.7	0	0	NFSC	708
7-2	#1	P at $L/4$	0.7	$17.5b_s$	0	NFSC	431
7-3	#1	P at $L/4$	0.7	$18.5b_s$	0	NFSC	403
7-4	#1	P at $L/4$	0.7	$18.6b_s$	0	NFSC	398
7-5	#1	P at $L/4$	0.7	$19.5b_s$	0	NFSC	NO
7-6	#1	P at $L/4$	0.7	0	$L/4$	NFSC	556
7-7	#1	P at $L/4$	0.7	0	$L/8$	NFSC	630
7-8	#1	P at $L/4$	0.7	-	-	iso834	490
7-9	#1	P at $L/4$	0.7	-	-	unif	376
8-1	#2	uniform	0.7	0	0	NFSC	548
8-2	#2	uniform	0.7	$7.5b_s$	0	NFSC	385
8-3	#2	uniform	0.7	$8.0b_s$	0	NFSC	367
8-4	#2	uniform	0.7	$8.1b_s$	0	NFSC	360
8-5	#2	uniform	0.7	$8.2b_s$	0	NFSC	348
8-6	#2	uniform	0.7	$8.3b_s$	0	NFSC	329
8-7	#2	uniform	0.7	$8.4b_s$	0	NFSC	NO

Table 4: (continued)

Case	beam	Load type	μ_0	$\triangle x$ (m)	$\triangle y$ (m)	Fire	T_{LTB} ^{o}C
8-8	#2	uniform	0.7	-	-	iso834	426
8-9	#2	uniform	0.7	-	-	unif	281

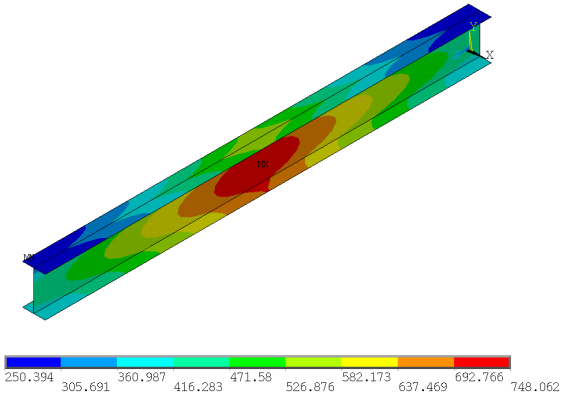

Figure 1: Temperature distributions within a steel ceiling beam subjected to a flame impinged localized fire [7]

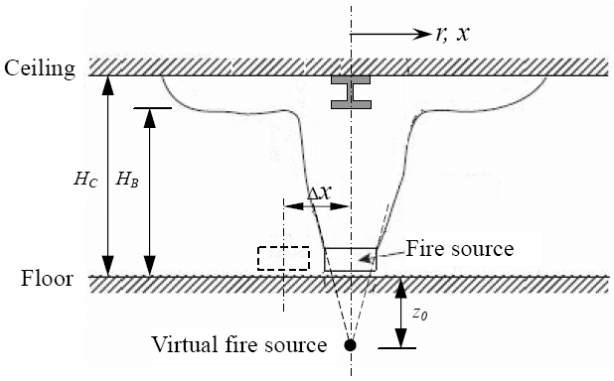

(a)

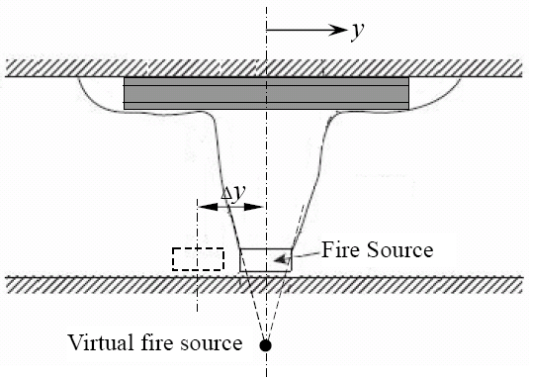

(b)

Figure 2: Illustration of the model used in investigated cases

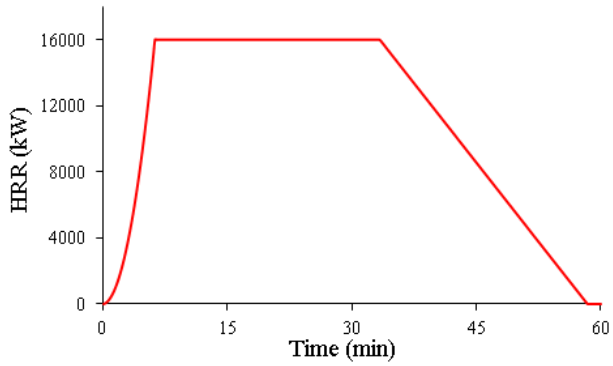

Figure 3: Heat release rates for the investigated localized fire

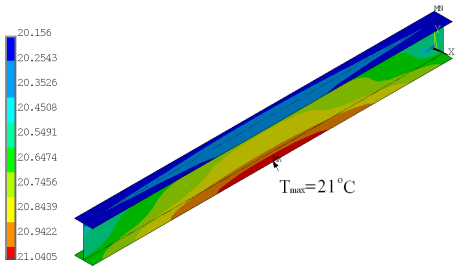

(a) early developing phase, at 120s

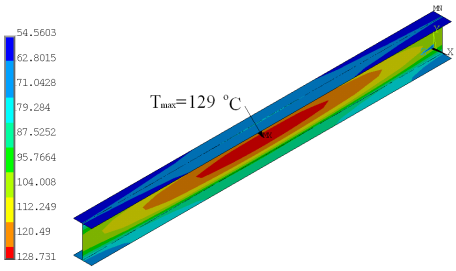

(b) developing phase end, at 380s

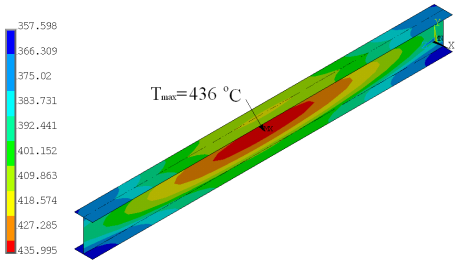

(c) steady burning end, at 2000s

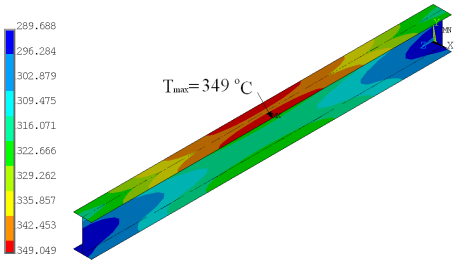

(d) decaying phase, at 3000s

Figure 4: Steel temperature distribution within a steel beam at different phases in a NFSC fire (case 3-7)

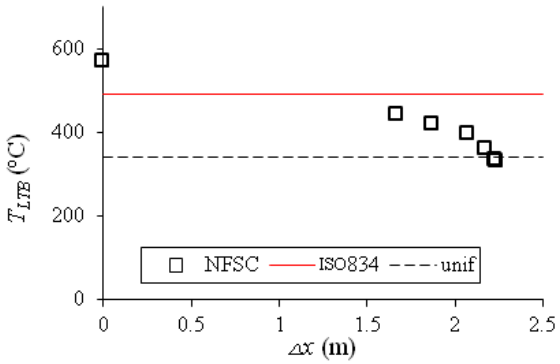

(a) uniform load, $\mu_0 = 0.7$ (b) Mid-span point load, $\mu_0 = 0.7$

Figure 5: The effect of $\triangle x$ on T_{LTB}

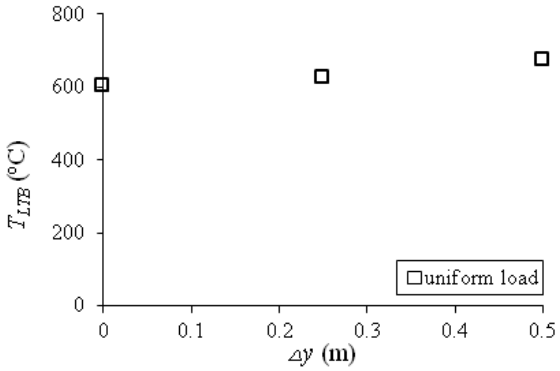

(a) uniform load, $\mu_0 = 0.7$

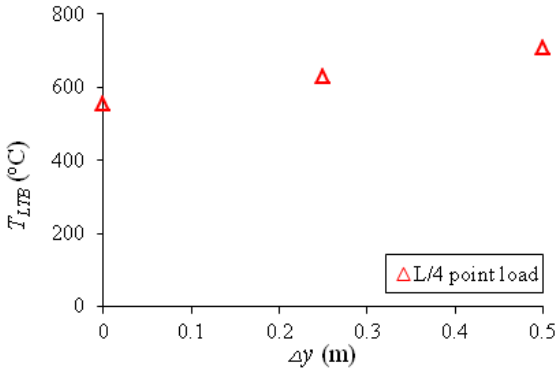

(b) Point load at quarter length, $\mu_0 = 0.7$

Figure 6: The effect of $\triangle y$ on T_{LTB}

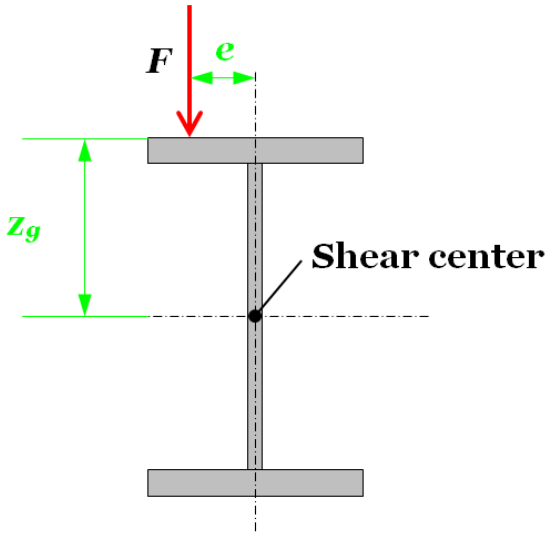

Figure 7: Schematic of load position on beam section

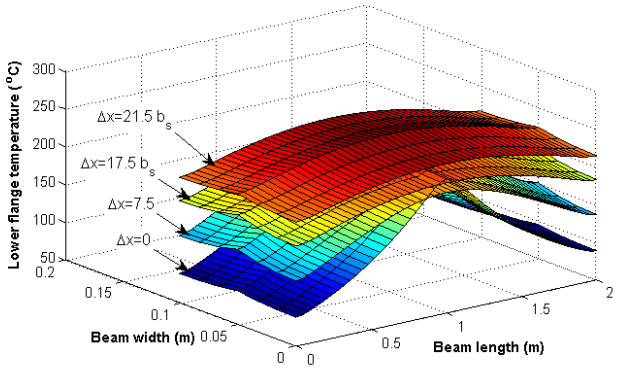

(a) Lower flange

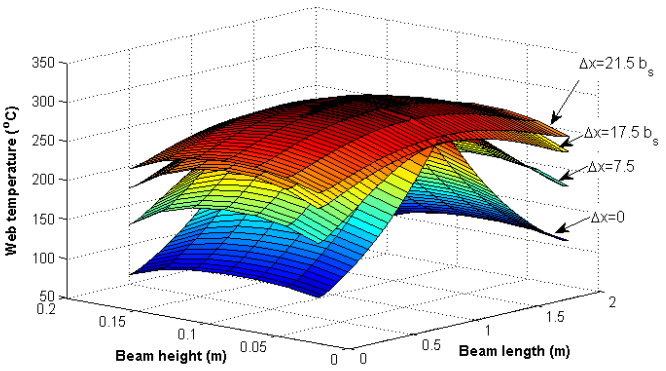

(b) Web

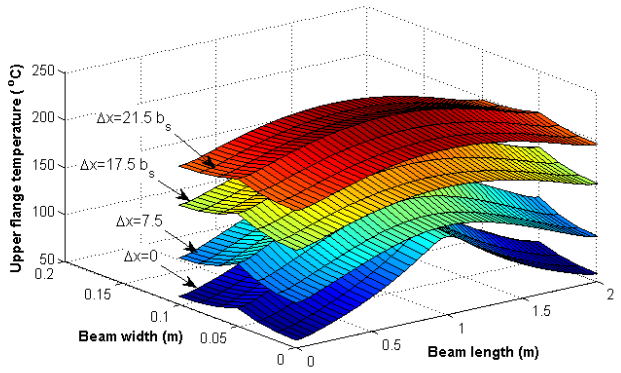

(c) Upper flange

Figure 8: Effect of $\triangle x$ on temperature distributions within different parts of beam (beam 1, the maximum steel temperatures for different cases are the same and equal to 300 ^{o}C)

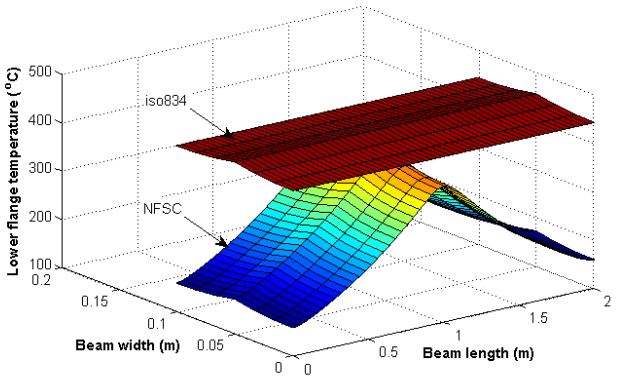

(a) Lower flange

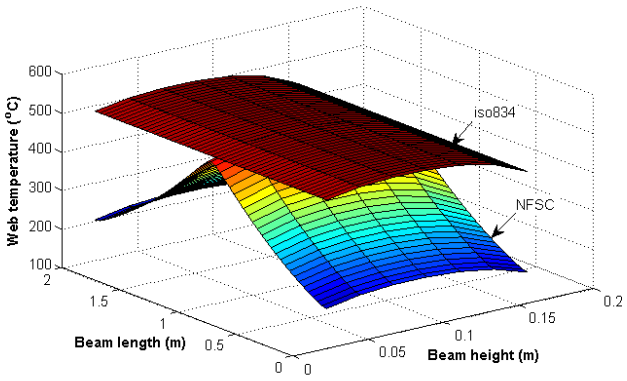

(b) Web

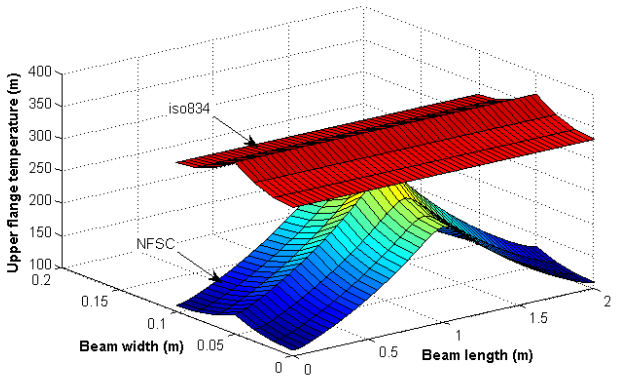

(c) Upper flange

Figure 9: Temperature distributions within different parts of beam 1 subjected to a NFSC fire (case 1-1), and the standard ISO834 fire (case 1-6). The maximum steel temperatures for the NFSC and ISO834 fires are the same and equal to 503 ^{o}C.

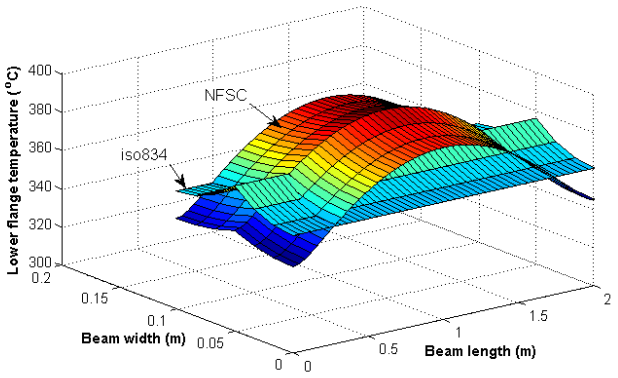

(a) Lower flange

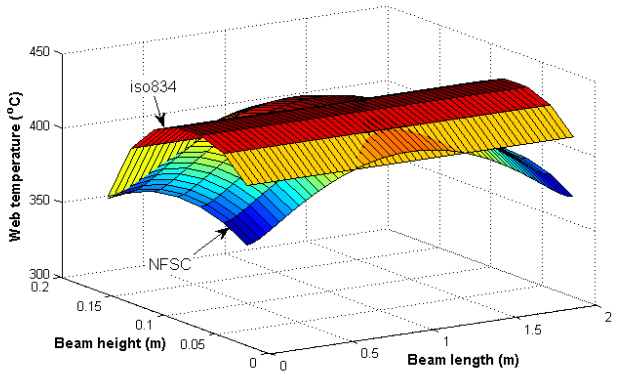

(b) Web

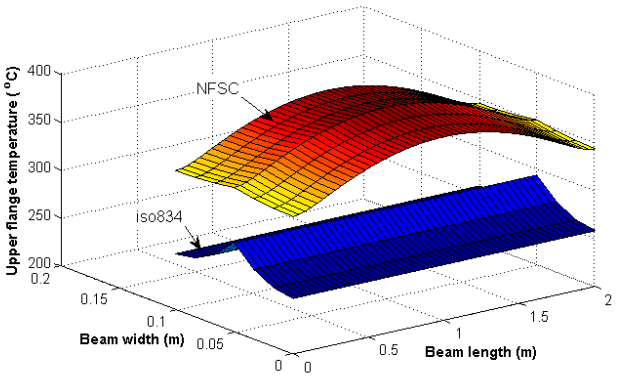

(c) Upper flange

Figure 10: Temperature distributions within different parts of beam 1 subjected to the NFSC fire (case 3-7) , and the standard ISO834 fire (case 3-10). The maximum steel temperatures for the NFSC and ISO834 fires are the same and equal to 429 ^{o}C.

(a) Cooling phase, failed

(b) Heating phase, not fail

Figure 11: Temperature distributions within beam #1 subjected to a NFSC fire (case 5-11) at heating and cooling phases

(a) Cooling phase, failed

(b) Heating phase, not fail

Figure 12: Temperature distributions within beam #1 subjected to the NFSC fire (case 6-6) at heating and cooling phases